Research Article | Vol. 12, No. 11 / 1 Nov 2021 / Biomedical Optics Express 7185
Biomedical Optics EXPRESS

In vivo fluorescence molecular imaging of the vascular endothelial growth factor in rats with early diabetic retinopathy

LU ZHANG,[1,2,3,7] YUNHE DING,[1,2,3,7] XINJIAN CHEN,[4,7] DEHUI XIANG,[4] FEI SHI,[4] YANYUN CHEN,[5] SHENSHEN YAN,[5] XINYUAN ZHANG,[5] JIE TIAN,[3] SOBHA SIVAPRASAD,[6] YANG DU,[3,8] ZHI YANG,[1,2,9] AND BEI TIAN[5,10]

[1]*School of Biomedical Engineering, Capital Medical University, Beijing, 100069, China*
[2]*Beijing Key Laboratory of Fundamental Research on Biomechanics in Clinical Application, Capital Medical University, Beijing, 100069, China*
[3]*CAS Key Laboratory of Molecular Imaging, The State Key Laboratory of Management and Control for Complex Systems, Institute of Automation, Chinese Academy of Sciences, Beijing, 100190, China*
[4]*School of Electronics and Information Engineering and the State Key Laboratory of Radiation Medicine and Protection, Soochow University, Jiangsu, 215006, China*
[5]*Beijing Tongren Eye Center, Beijing Tongren Hospital, Capital Medical University, Beijing, 100730, China*
[6]*NIHR Moorfields Biomedical Research Centre, Moorfields Eye Hospital, London, EC1 V 2PD, UK*
[7]*These authors contributed equally to this work*
[8]*yang.du@ia.ac.cn*
[9]*zhiyang@ccmu.edu.cn*
[10]*tianbei@ccmu.edu.cn*

Abstract: Anti-vascular endothelial growth factor (anti-VEGF) therapy is effective for reducing the severity level of diabetic retinopathy (DR). However, it is difficult to determine the *in vivo* spatial and temporal expression of VEGF in the DR retina at an early stage. Here, we report a quantitatively fluorescence molecular imaging and image analysis method by creating a VEGF targeted fluorescence imaging probe, which can potentially detect and predict anti-VEGF treatment response. Moreover, the ex vivo multiscale fluorescence imaging demonstrated the spatial correlation between VEGF relative expression and vascular abnormalities in two and three dimensions. It revealed that VEGF was mainly abnormally expressed at the bifurcation of the microvessels, which advances the knowledge of the DR progression by molecular fluorescence imaging. Our study has the potential to achieve early detection of DR disease, provide more insight into understanding anti-VEGF treatment, and may help stratify patients based on the molecular imaging of retinal VEGF.

1. Introduction

According to the global diabetes report released by the World Health Organization, the number of diabetic patients worldwide has exceeded 422 million, accounting for 8.5% of the global population [1]. China has 100 million diabetic patients, which is the largest number in the world. Diabetic retinopathy (DR) is one of the most common and serious complications of diabetes, and is also one of the most important diseases that can cause blindness in the working age group [2,3]. The optimal therapeutic opportunity for DR is the non-proliferative DR (NPDR) stage [4,5]. Once DR develops into the proliferative phase, irreversible structural damage occurs and the rate of blindness increases [6,7]. At present, the effective evidence-based treatments for DR are retinal photocoagulation, vitrectomy, anti-vascular endothelial growth factor (anti-VEGF)

#439446 https://doi.org/10.1364/BOE.439446
Journal © 2021 Received 11 Aug 2021; revised 15 Oct 2021; accepted 20 Oct 2021; published 29 Oct 2021

Biomedical Optics EXPRESS

treatment, and glucocorticoid treatment. Anti-VEGF therapy is mainly used in the treatment of diabetic macular edema and proliferative DR before surgery [8,9]. Although the pathogenesis of DR is multifactorial, VEGF is a critical factor for pathological angiogenesis [10–12]. It can induce vascular endothelial cell proliferation and migration, change the expression of adhesion molecules in vascular endothelial cells, promote the generation of reactive oxygen species, and increase retinal capillary permeability. When VEGF is inhibited by anti-VEGF agents, the severity level of DR is significantly reduced, suggesting that retinal VEGF is the main driver of DR lesions, especially retinal hemorrhage, intraretinal microvascular abnormalities, and retinal neovascularization [13–15]. Moreover, retinal hemorrhage represents the sequela of structural changes. Intraretinal microvascular abnormality (IRMA) is a structural alteration induced, at least in part, by VEGF, which is one of the defining hallmark features of NPDR [16]. At this time, anti-VEGF treatment is clinically recommended for diabetic macular edema and proliferative diabetic retinopathy. Several reports show that even in the early stage of DR, the retina have both increased expression as well as accentuated response to VEGF [17–19]. Such expression and response could theoretically result in a positive feedback loop [20] that might eventually induce retinal ischemia and VEGF expression to stimulate intraocular neovascularization. This hypothesis raises the intriguing possibility that anti-VEGF treatment might prevent retinopathy progression in the early non-proliferative stage [21].

In addition, it is difficult to distinguish anti-VEGF treatment responders from non-responders. We believe that if we can image the expression of VEGF in the retina, we can localize whether the drug has reached the DR lesions and accurately stratify patients and offer precision medicine. The current diagnosis of DR is mainly based on fundus photography and fluorescein angiography [22–24]; however, these methods only detect structural sequelae, and the sensitivity is lower than that of molecular imaging technology. Moreover, they cannot quantitatively detect and monitor the expression level of VEGF as a key pathogenic target. Increased VEGF levels in the vitreous are a surrogate marker of retinal VEGF, but vitreous fluid biopsies [25–27] cannot be used to monitor disease in routine clinical practice. Currently, it is not possible to clinically visualize and quantify the expression of VEGF molecules *in vivo*.

The confocal scanning laser ophthalmoscope (cSLO) is a common instrument used for fluorescein angiography and fundus autofluorescence, and is equipped with a blue laser exciter. Hence, cSLO can be utilized for *in vivo* molecular imaging of VEGF expression. The structure of the eye provides a unique platform for light-based molecular imaging, and the high sensitivity and specificity of the molecular imaging probes make them highly suitable for the detection of VEGF expression, as observed in DR. Several applications of *in vivo* molecular imaging of retinal diseases have been reported. For example, Cordeiro et al. studied retinal nerve cell apoptosis *in vivo* with fluorescent-labeled annexin 5 probes [28], Further, Meyer et al. investigated the fluorescent probes for choroidal neovascularization imaging based on cSLO [29], and Sun et al. revealed increased expression of vascular endothelial growth factor receptor 2 in the retinal capillary endothelia of diabetic rats compared to controls *in vivo* [30].

In this study, we aimed to design a fluorescein isothiocyanate (FITC)-labeled VEGF antibody fluorescence probe (Ranibizumab-FITC) with high selectivity, sensitivity, and stability, combined with advanced molecular imaging and medical image analysis techniques to conduct quantitative imaging and analysis of VEGF expression in the rat retina in early DR *in vivo*. *Ex vivo* fluorescence imaging of retinal flatmount analysis was then performed to characterize VEGF expression to verify the *in vivo* observation (Fig. 1). Our study demonstrates a reliable tool for the dynamic, minimally invasive, and quantitative analysis of VEGF relative expression in DR, which provides a clinical decision tool for retinal specialist to provide precise treatment.

Biomedical Optics EXPRESS

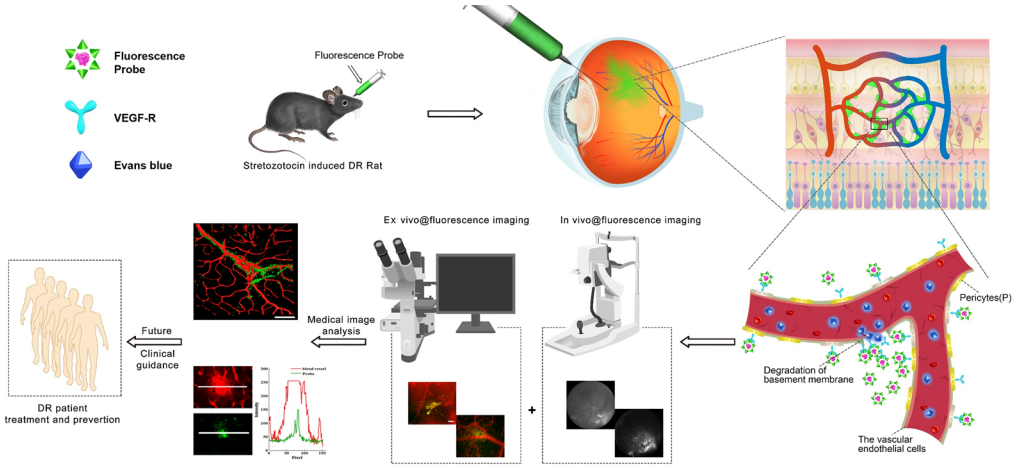

Fig. 1. Schematic illustrations of the study design and experimental procedures are shown. BN rats with diabetic retinopathy (DR) were enrolled in the study, and then received an intravitreous injection with a sterile Ranibizumab-fluorescein isothiocyanate (FITC) fluorescence imaging probe, which was synthesized by covalently binding of VEGF antibody ranibizumab with fluorescent dye FITC. The *in vivo* VEGF-targeted fluorescence imaging was identified mainly in the affected vascular area of the retina. In order to validate the *in vivo* imaging results and further characterize the detailed molecular and cellular changes in the diseased area, the retinal flatmounts were further examined using different types of fluorescence imaging equipment at multiple scales. Furthermore, medical image analysis was applied to analyze and quantify VEGF molecular expression. (VEGF-R, Vascular endothelial growth factor receptor)

2. Material and methods

2.1. Fluorescence probe

In this study, ranibizumab (recombinant humanized IgG1 kappa isotype monoclonal antibody fragment designed, Lucentis, Novartis, Basel, Switzerland) was covalently attached to the fluorescent dye (FITC) to synthesize the VEGF fluorescence probe. Antibodies were labeled under sterile conditions. Briefly, 1 mg of FITC and 2 mg of ranibizumab were dissolved in 2 mL of dimethyl sulfoxide. After 0.1 mL of three ethylamine was added, it reacted at room temperature. Ranibizumab was covalently attached to FITC to synthesize the VEGF fluorescent probe (Ranibizumab-FITC). After purification with high-performance liquid chromatography and fluorescence spectroscopy, the probe was dialyzed in a dialysis bag and lyophilized for 24 h. Solutions were lyophilized and subsequently stored at 4°C. When the probe was applied to the animal, the labeled antibody was reconstituted with phosphate buffered saline (PBS) to a concentration of 10 μg/μL for intravitreal injection (5 μL).

2.2. Animal models

Six to eight-week-old male Brown Norway (BN) rats were purchased from Vital River Laboratory Animal Technology Corporation (Beijing, China). All procedures were carried out in accordance with the approved guidelines, and the protocol was approved by the Animal Welfare Committee of Capital Medical University (Permit No: AEEI-2019-102). The rats were divided into two groups (n = 6 for the control group and n = 6 for the DR group). After 16 h of overnight fasting, the DR group was intraperitoneally injected with streptozotocin (STZ) (60 mg/kg in 5 mM, pH 4.3, citrate buffer; Sigma-Aldrich Corp. St. Louis, MO, USA) to induce diabetes. The control

Biomedical Optics EXPRESS

group was intraperitoneally injected with an equal amount of buffer. Animals with blood glucose levels higher than 13.8 mmol/L at 72 h after STZ injection were considered diabetic [31]. Body weight and blood glucose levels were measured every two weeks. Animals were maintained in an air-conditioned room under a 12 h light/dark cycle and were given *ad libitum* access to water and food.

2.3. In vivo imaging

After being reared for eight weeks, the STZ-induced DR rats were anesthetized with 1% pentobarbital sodium (40 mg/kg, EMMX Biotechnology LLC). The pupils of both eyes were dilated with 0.5% tropicamide and 2.5% phenylephrine hydrochloride (Mydriaticum Stulln, Pharma Stulln, Germany). Each eye received a single intravitreal injection of molecular probes (5 μL, 10 mg in 1 mL of PBS). High-resolution images of the fundus were captured using a cSLO (Spectralis HRA; Heidelberg Engineering, Heidelberg, Germany). Fluorescence images with the same settings were taken before dye injection and at different time points post-injection (0, 6, 24, and 72 h). For the entropy-based image segmentation, Renyi entropy was performed to provide further quantitative image analysis of *in vivo* VEGF imaging [32].

2.4. Ex vivo visualization and three-dimensional image analysis

For further visualization of the fluorescence probe in the DR retina, retinal flatmounts were prepared for *ex vivo* fluorescence imaging at multi-scale levels. After the *in vivo* imaging experiment, all rats were euthanized using 1% sodium pentobarbital (40 mg/kg, intraperitoneal injection). Microvessel networks were labeled by intravenous injection of Evans blue (30 g/L dissolved in saline solution), with 0.2 ml for each rat. Ten minutes after the injection, both eyes were enucleated. The retinas were separated and cleaned with PBS, and then immersed in 4% polyformaldehyde solution to prepare a flat specimen. Fluorescence was imaged using filter sets for excitation and emission at 470/40 and 525/50 nm for FITC and 550/25 and 605/70 nm for Evans blue (FITC: green; EB: red). Subsequently, the retinal flatmounts were analyzed using an inverted fluorescence microscope (LeicaM165FC/205FA, Leica), dual-wavelength confocal microscopy (Cellvizio, Mauna Kea Technologies), and confocal fluorescence microscopy (TCS SP5, Leica).

The image series obtained from the confocal microscope was reconstructed into a 3D model using Amira 5.2.2 (Visage Imaging, San Diego, CA). The surface rendering method was used to visualize the VEGF expression and Evans blue dying, which demonstrated the complex spatial relationships of VEGF and vascular lesions by manually setting the threshold of the iso-surface. The distribution of the VEGF fluorescence probe was analyzed in three dimensions.

2.5. Western blot

Eight retinas from the DR and normal groups were randomly chosen for protein extraction to detect VEGF by western blotting. From each group, 50 μg of protein was extracted and dissolved in 10% twelve alkyl sulfate polyacrylamide gel and then transferred to the polyethylene difluoride film. The samples were eluted, sealed with 5% skimmed milk powder, and diluted with VEGF to 1: 1000 (Abcam, Cambridge, MA, USA). The samples were incubated overnight at 4°C. On the second day of the experiment, the antibodies were eluted and were then incubated with goat anti-rabbit antibody peroxidase-coupled antibody. The dilution ratio was 1: 2000 (Abcam, Cambridge, MA, USA) and incubation occurred at room temperature for 2 h. Using enhanced chemiluminescence reagents (Amersham Biosciences, Piscataway, NJ, USA), protein signals were visualized, and multi-spectral imaging systems (Biospectrum AC Chemi HR 410, UVP, LLC, Upland, CA, USA) were used for imaging. The samples were then eluted again and the monoclonal antibody beta-tubulin (1: 2000 dilution, BD Biosciences, San Jose, CA, USA) was used as an internal reference. The optical density of the target protein was measured using

Biomedical Optics EXPRESS

Image J software (National Institute of Health, Bethesda, MD, USA) and standardized using beta-tubulin. Fluorescent images were acquired using a high-sensitivity digital camera connected to a computer-assisted image analysis system.

2.6. Quantitative real time-polymerase chain reaction (qRT-PCR)

Three rats were randomly chosen from the DR group and normal group respectively. Each group had six retinas. The RNAs were extracted by Trizol method, and then reverse transcription to obtain cDNA. The expression of VEGFA was detected by qRT-PCR. 2-ΔΔCT method was used to get a quantitative description of the gene expression. Premers used in this study were as follows: Gapdh(F: 5'-TTCAACGGCACAGTCAAGG-3', R: 5'-CTCAGCACCAGCATCACC-3'); VEGFA(F:5'-TATATCTTCAAGCCGTCCTGTG-3',R:5'-TTGTTCTATCTTTCTTTGGTCTGC-3').

2.7. Cytotoxicity of the fluorescence probe

Human umbilical vein endothelial cells (HUVECs) were obtained from Capital Medical University. The cells were cultured in normal dulbecco's modified eagle medium (DMEM), with 10% fetal bovine serum (FBS) and 1% penicillin/streptomycin at 37°C under 5% CO_2. Cell proliferation was assessed using the Cell Counting Kit 8 (CCK-8) assay; cells were seeded in 96-well plates and infected with the fluorescent probe. After 1 h of adsorption, the cells were washed once and refed with DMEM culture medium supplemented with 10% FBS and incubated at 37°C. Cell viability was assayed at 36 h post-infection. According to the manufacturer's instructions, 10% CCK-8 solution (Engreen, Beijing, China) was added to each well and the absorbance was determined at 450 nm after 2 h of incubation using an ELISA microplate reader (BioTek Instruments, Winooski, VT, USA). Uninfected cells were used as the negative control group, and the assay was repeated at least three times.

2.8. Binding affinity test

The interaction of ranibizumab or ranibizumab-FITC with recombinant rat (rr) $VEGF_{164}$ (P. pastoris-expressed, Solarbio) were determined by surface plasmon resonance (SPR) technology using a Biacore T200 unit (GE Healthcare). All the SPR-based materials were purchased from GE Healthcare. HBS-EP+ (10 mM HEPES, 150 mM NaCl, 3 mM EDTA, 0.05% P20, pH 7.4) was used as the running buffer. Briefly, rr $VEGF_{164}$ was immobilized on CM5 chips (GE Healthcare) to a level of approximately 300 resonance units (RU) following standard procedures. A flow cell without immobilized protein served as a non-specific binding control. Antibodies were injected over the sensor surface at 30 μL/min at five concentrations (1000, 500, 250, 125, 62 nM). The chip surface was regenerated after each cycle by injecting 1 M NaCl for 30s. KD was determined using the "kinetics" model in the Biacore T200 evaluation software version 2.0.

2.9. Immunofluorescence

The retinas were analyzed by immunofluorescence. Briefly, normal and DR rats were euthanized with 1% sodium pentobarbital (40 mg/kg, intraperitoneal) and their eyes were enucleated. The retinas were separated, cleaned with phosphate buffered saline, and embedded in paraffin after being fixed in fresh 4% paraformaldehyde. Sections that were 10 μm in thickness were mounted on a glass slide. After removing the paraffin and rehydrating the sections, the sections were blocked and incubated with a primary antibody against VEGF-A (Proteintech, Rosemont, IL, USA) at 4°C overnight and were then incubated with a secondary antibody conjugated to CY5.5 (Abcam, Cambridge, MA, USA) at 37 °C for 2 h. Nuclei were stained with DAPI. The test of colocalization of the VEGF antibody and our probe was performed by incubating primary antibody against VEGF-A (Proteintech, Rosemont, IL, USA) together with the probe overnight.

Biomedical Optics EXPRESS

The second antibody was conjugated to Cy5.5. Fluorescent images were obtained using a confocal microscope (TCS SP5, Leica).

2.10. Statistical analysis

Statistical analyses were performed using Prism version 5.0 (San Diego, CA, USA). Data were analyzed using a Student's *t*-test. P-values < 0.05 were considered statistically significant.

3. Results

3.1. DR model establishment and the expressions of VEGFA validation in DR retina ex vivo

Compared with the normal group, all the rats in STZ-induced DR group had symptoms of diabetes. The blood glucose levels and body weights were measured at various time points in each group (Supplement 1, Fig. S1, A and B). As soon as 24 hours after STZ injection, the blood glucose increase significantly. This high blood glucose remained for 8 weeks. Meanwhile, the body weight decreased significantly eight weeks after injection. The rats in DR group also suffered from polydipsia, polyphagia and polyuria. To valid the successful modeling of DR, the western blot (Supplement 1, Fig. S2A) and quantitative real time - polymerase chain reaction (qRT-PCR) (Supplement 1, Fig. S2B) were further performed, which confirmed that the VEGFA expression in DR group was significantly higher than the normal control group at both RNA and protein level.

3.2. Binding property and biosafety of the VEGF targeting probe

The cytotoxicity test of ranibizumab-FITC probe showed no toxic effects of the fluorescence probe in viability of HUVECs (Supplement 1, Fig. S2C). Surface plasmon resonance (SPR) binding affinity test showed that ranibizumab and ranibizumab-FITC bind to recombinant rat (rr) $VEGF_{164}$ with KD values of 500 nM and 934 nM, respectively (Supplement 1, Fig. S2D). It indicates that the probe still maintains good biological activity and binding characteristics. Immunofluorescence of VEGF in the retina from paraffin sections also proved that the VEGF targeting property of the probe was retained. Excellent VEGF colocalization was demonstrated by the VEGF antibody and the fluorescence probe (Supplement 1, Fig. S2E).

3.3. In vivo characterization of VEGF expression using fluorescence imaging and image analysis

The *in vivo* imaging of the ranibizumab-FITC probe was performed on eight-week old DR rats and normal rats using Heidelberg Spectralis HRA (Heidelberg Engineering, Germany). Fluorescence images were captured before intravitreal injection of the fluorescence probe (Pre) and after the injection (0, 6, 24, and 72 h). No retinal abnormalities or fluorescent spots were detected in any of the groups before injection (Fig. 2(A), first column). Following intravitreal injection (0 h), strong homogenous fluorescence was visible at the injection site quadrant for all groups (Fig. 2(A), second column). In the normal group (Fig. 2(A), first row), 6 h after injection, the blood vessels showed low fluorescence, indicating that the probe did not enter the retinal blood vessels, but the retinal fluorescence increased significantly compared with that before injection. After 24 h, the fluorescence signal started to accumulate in the major retinal veins, indicating that the probe entered the venous system. Then, both the fluorescence spots and the retina intensity decreased at 72 h. In contrast, the fluorescence image of the ranibizumab-FITC probe showed different results in the DR rat model (Fig. 2(A), second row). A remarkably high fluorescence signal was observed in the retina 6 h after injection (white arrow). The fluorescence signal was still found in the target tissues 24 h later (white arrow). After 72 h, the fluorescence declined sharply. The images of DR rats with free FITC injection are shown in the third row of

Biomedical Optics EXPRESS

Fig. 2(A). After 6 h, the overall fluorescence intensity decreased sharply, and no specific area was fluorescent. After 24 h, the fluorescent dye had disappeared from the retinal circulation; the choroidal blood vessel fluorescence increased, and there was fluorescence aggregation at the optic disc at 72 h (white arrow). These results indicated that the ranibizumab-FITC probe developed in this study has the ability to achieve targeted imaging of VEGF and to locate the high VEGF expression region *in vivo*.

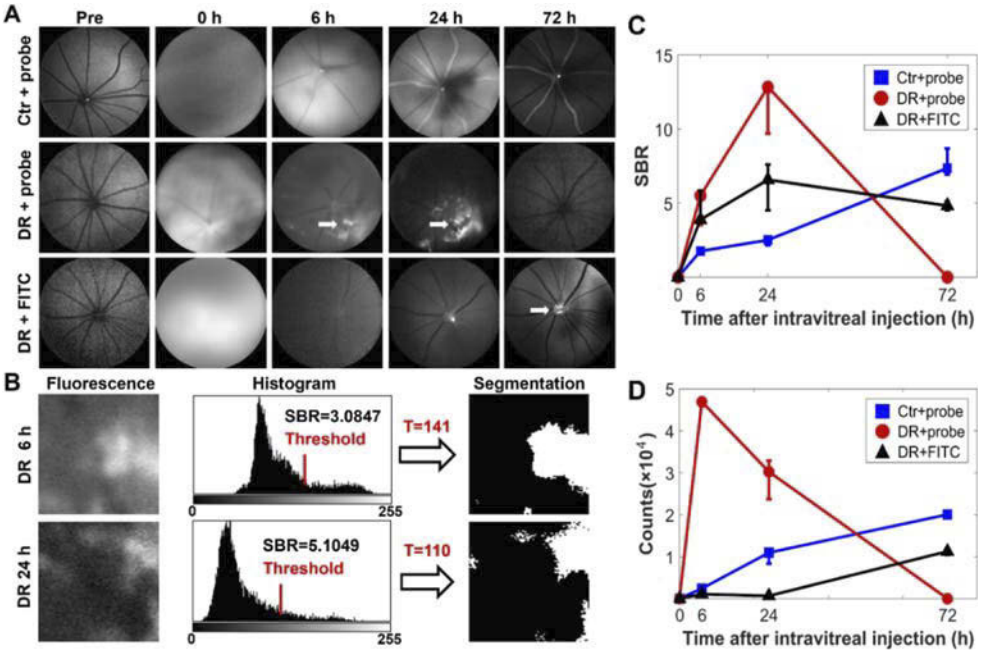

Fig. 2. *In vivo* fluorescence imaging and image analysis of VEGF expression. (A) *In vivo* fluorescence imaging over time in normal and diabetic retinopathy (DR) rats' eyes with intravitreal injection of ranibizumab- fluorescein isothiocyanate (FITC) and free FITC dye. After probe injection, a remarkably high fluorescence signal (pointed out by the white arrows) was observed in the retina at 6 and 24 h in the same lesion area as the DR model with ranibizumab-FITC injection. (B) Fluorescence images, histograms, and Renyi entropy threshold segmentation of the fluorescence positive regions in the DR + probe group. T = image segmentation threshold. (C) SBR after intravitreal injection of probes over time. (D) The fluorescence signal of the fluorescence positive area after intravitreal injection of probes over time. (Ctr, control)

Moreover, we used image segmentation to provide a more objective, precise, and quantitative description of the fluorescent signals indicating the VEGF expression level. In this study, Renyi entropy, which is an automatic and global segmentation method, was performed to realize the automatic segmentation of the VEGF expression region and measurement of VEGF. Figure 2(B) shows the fluorescence images, histograms, and Renyi entropy threshold segmentation of the fluorescence-positive regions in the DR model with the ranibizumab-FITC probe group. A small area of 100 × 100 pixels was selected from the 6 h and 24 h images. The segmentation results showed that the stationary bonded probes showed higher SBR (Signal to background ratio) at 24 h after injection. The range of gray level distribution in the 24 h image was much wider, indicating higher image contrast. Figure 2(C) shows the SBR of the images in the three groups at each time point after injection. Only in the DR model + probe group did the SBR peak at 24 h. Figure 2(D) shows the area of fluorescent spots in the three groups at each time point after

Biomedical Optics EXPRESS

injection. The probes in the normal group accumulated in the veins; thus, the fluorescent spots slightly increased over time. In contrast, high VEGF levels were found in DR retinas. Our probes immediately converged to retinal lesions with notable fluorescent signals (6 h) and then free probes were gradually metabolized (24 h), which led to a drop off of the fluorescence area.

3.4. *Imaging of VEGF expression and vascular abnormalities at multiscale levels ex vivo*

In order to validate the *in vivo* imaging results and further characterize the detailed molecular and cellular changes in the diseased area in the DR retina, the retinal flatmounts were further examined using three different types of fluorescence imaging equipment with different imaging scales. Our ranibizumab-FITC probe emits green fluorescence when excited by blue light. At the same time, the blood vessels were perfused with Evans blue (EB), which emits red fluorescence when excited. Using inverted fluorescence microscopy, the normal retinal fluorescence images are shown in the first rows of Fig. 3(A) and Figure S3. The vascular structure was clear, and the probe fluorescence signal could not be obtained due to the low expression level of VEGF in normal retinal samples. Interestingly, we unexpectedly identified the micro-vascular change, IRMA, which is one of the defining features of NPDR. The second and third rows in Fig. 3(A) show two typical images of IRMA in DR retinas, revealed by EB staining, which are co-localized with the VEGF-positive green fluorescence signal. These results indicate that our fluorescence probe performs quite well in identifying VEGF expression in specific retinal lesions, such as IRMA in NPDR.

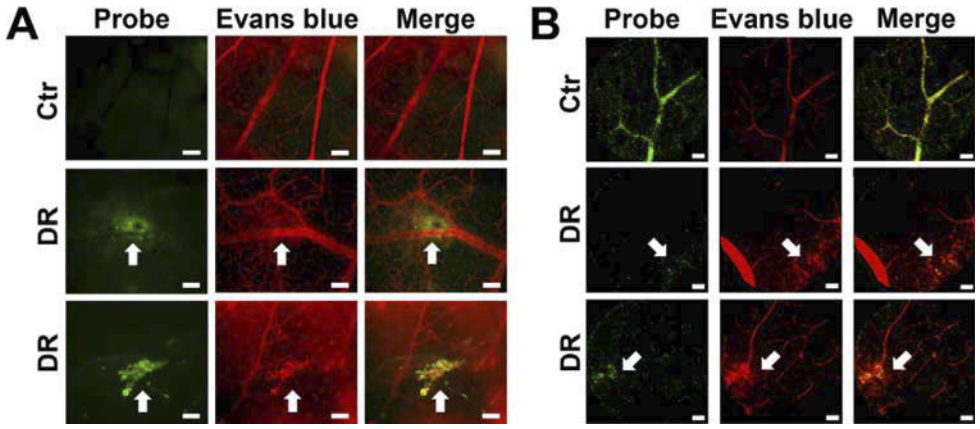

Fig. 3. *Ex vivo* analysis of fluorescent images of VEGF in retinal flatmounts. (A) Retinal flatmount images under inverted fluorescence microscopy. The first row is from a normal retina (bar = 100 μm). The second (bar = 100 μm) and third rows (bar = 50 μm) are from diabetic retinopathy (DR) retinas, and the white arrows indicate intraretinal microvascular abnormalities and VEGF positive areas. (B) Retinal flatmount images under confocal laser microscopy cellvizio (bar = 50 μm). The first row is from a normal retina. The second and third rows are from DR retinas, and the white arrows indicate the abnormal capillaries and VEGF positive staining. (Ctr, control)

Moreover, dual-wavelength confocal microscopy (Cellvizio, Mauna Kea Technologies) was also utilized, which can provide real-time imaging of vascular microarchitecture with high sensitivity and resolution. The imaging results are shown in Fig. 3(B) and Figure S4. The first row of Fig. 3(B) shows the detailed and complete retinal vascular network in the normal control group injected with the ranibizumab-FITC probe and stained with EB, and no vascular abnormality was found. The retinal vascular networks in DR rats are shown in the second and

Biomedical Optics EXPRESS

third rows of Fig. 3(B). The EB staining identified the early microvascular abnormities (in red color), where they were colocalized with high VEGF expression (in green color) marked by white arrows.

Confocal microscope imaging was also performed on normal and DR rats, and the data are shown in Fig. 4(A) and Figure S5. In the DR model, multiple dilated ends of capillaries were fused into a hemangioma with a larger diameter (white arrow) due to the increase in vascular wall permeability. Capillary bed occlusion was observed using EB staining. These features were absent in the retinas of normal rats. In particular, the hemangioma showed a remarkable green fluorescence signal for VEGF expression indicated by the white arrow, while no obvious probe signal could be found in the normal retina. The above data suggest that higher levels of VEGF expression usually occur in the abnormal retinal area, indicating the underlying cause and effect correlation. Compared with the DR group, the SBR in normal samples was significantly lower (Fig. 4(B)). A further quantitative description is given by a profile plot of the lines marked in Fig. 4(C). The pixel intensities of the two white lines in the vascular and probe images are shown next to the images. The white arrows indicated that the probe intensity in the hemangioma is much higher than in the normal retina.

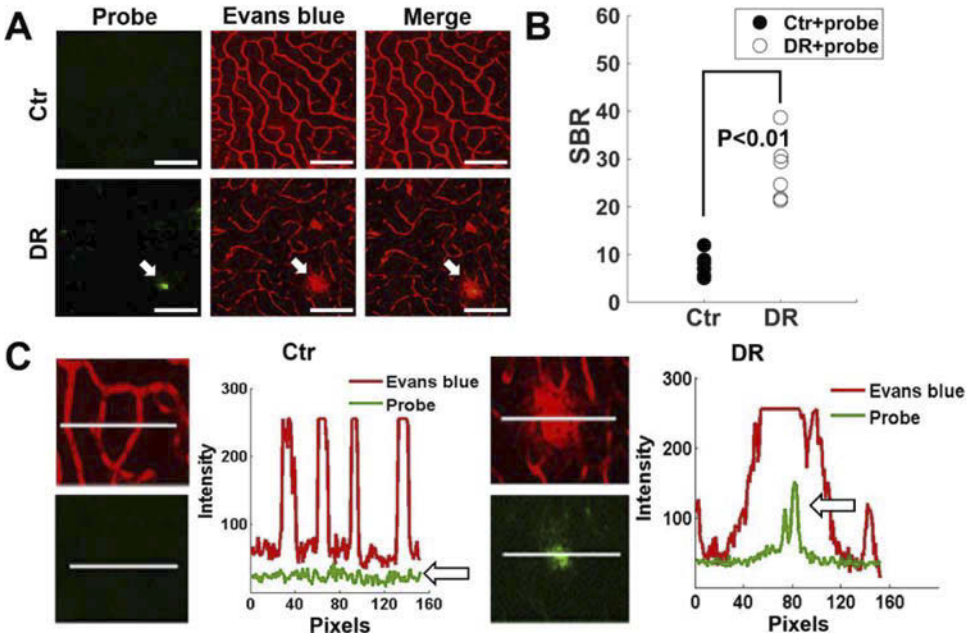

Fig. 4. *Ex vivo* analysis of fluorescent images of VEGF in retinal flatmounts. (A) Retinal flatmount images were imaged using a confocal fluorescence microscope (bar = 50 μm). The first row is the normal model. The second row is the DR model. (B) Probe fluorescence SBR in the normal (n = 6) and DR retinas (n = 6). (C) Profile plot of the lines marked in the images of normal and DR retinas. The pixel intensity of the two white lines in the vascular and probe images is shown next to the images. (Ctr, control)

3.5. *Spatial correlation between VEGF expression and vascular abnormalities at the early stage of DR*

In order to further investigate the correlation between VEGF-positive expression and the diseased blood vessels, an image series obtained from confocal fluorescence microscopy was further reconstructed into a three-dimensional (3D) model (Fig. 5 and Supplement 1, Fig. S6). The

Biomedical Optics EXPRESS

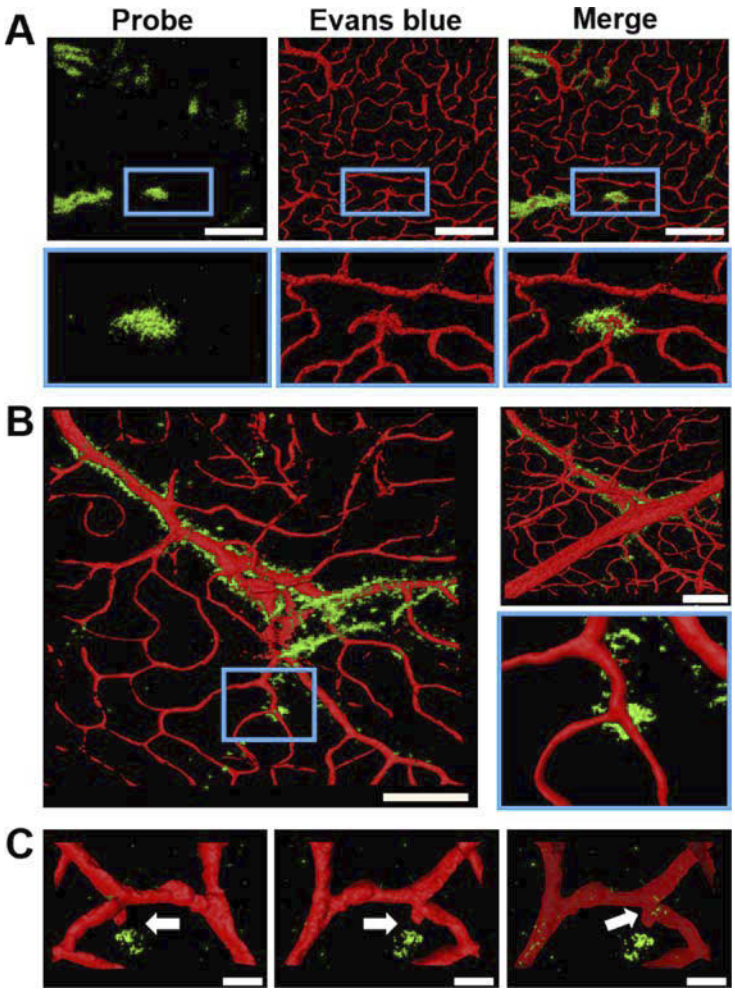

Fig. 5. Three-dimensional (3D) reconstruction of confocal fluorescence microscope images of VEGF in the vascular abnormities in diabetic retinopathy (DR) retinas. (A) 3D surface rendering of imaging probes (green color) and blood vessels (red color). There is obvious binding of fluorescence probes surrounding the vascular abnormalities. The enlarged view of the area outlined in the blue boxes above are shown in the second row. The probes were aggregated and bound to the dilated capillary, indicating high VEGF expression (bar = 100 μm). (B) 3D view of the lesion area with probe binding to the surface of the vessel. The upper right image is the opposite view of the left image. The lower right image is the enlarged image of the blue box (bar = 50 μm). (C) 3D view of capillary dilation. The capillary with obvious vessel wall dilatation is pointed out by the white arrow in the front view (left) and opposite view (middle). Meanwhile, a remarkable amount of VEGF accumulated in the direction of the capillary wall expansion, indicating that VEGF may have induced this capillary angiogenesis. The transparent view of the capillary (right) shows VEGF in the capillary indicated by white arrow (bar = 15 μm). (Ctr, control; DR, Diabetic retinopathy.)

distribution of the VEGF fluorescence probe was analyzed in three dimensions. Interestingly, we found that there was obvious aggregation of fluorescence probes surrounding the vascular abnormalities shown in the first row (Fig. 5(A)). The enlarged views of the fluorescence areas are shown in the blue box in the second row. This revealed that the green fluorescence was

Biomedical Optics EXPRESS

mainly aggregated and bound to the dilated capillary, indicating that high VEGF expression was mainly located in the lesioned blood vessel areas. The 3D model of the DR retina is displayed from different angles and magnifications in Fig. 5(B). VEGF probes mainly bind to the surface of abnormal blood vessels. The fluorescent probe bound specifically to the bifurcation of the microvessels, which validated that early DR is likely to start from the bifurcation of the microvessels. Moreover, we found that the walls of some capillaries bulged outward in the early stage of DR. Figure 5(C) shows the 3D model of a small section of the capillary with obvious vessel wall dilatation pointed out by the white arrow. Meanwhile, a remarkable amount of VEGF accumulated in the direction of the capillary wall expansion, as shown in the front view (left) and opposite view (middle), indicating that VEGF may induce capillary angiogenesis. In the transparent view of the capillary (right), we also found a small amount of VEGF expression located inside the capillary dilation area, as indicated by the white arrow, which may also play a role in vascular angiogenesis.

4. Discussion

Noninvasive and quantitative detection of VEGF plays a significant role in the early identification, diagnosis, and intervention of DR from the non-proliferative to the proliferative stage, which may prevent the progression of the disease, improve or maintain visual function, and reduce the incidence of blindness. However, there are currently no accurate imaging methods to visualize and quantify early VEGF elevation during DR progression. In this study, we effectively developed a targeted fluorescence probe combined with molecular fluorescence imaging to assess VEGF expression in the retina *in vivo*. Compared with other widely used anti-VEGF agents [33–35], such as bevacizumab and afibercept, ranibizumab lacks the Fc region, allowing it to avoid Fc recycling and make it significantly smaller than the full-size antibody. Smaller size is thought to facilitate easier penetration into the retina and faster clearance systemically, and it may also expedite clearance from the vitreous [34,36]. In this study, we implemented an accurate VEGF-targeted imaging. In combination with vascular fluorescent imaging stained with EB, our probe makes it possible to definitively localize VEGF expression in abnormal vascular networks with proliferative tendencies. Therefore, the correlation between VEGF and the pathological changes of microvessels at multiscale levels was further characterized. More generally, we successfully demonstrated the 3D relationship between VEGF relative expression and vascular abnormalities at the early stage of DR.

To the best of our knowledge, there are few studies on *in vivo* imaging and the pharmacokinetics of VEGF in NPDR rats [37,38]. Traditional DR imaging is mainly based on fundus photography, fluorescein angiography, and optical coherence tomography. These imaging modalities identify the sequelae of abnormal retinal microvasculature. Hence, early quantitative detection of VEGF concentration is urgently needed. In this study, clinical cSLO was used to dynamically monitor the *in vivo* biodistribution of the ranibizumab-FITC probe in a rat model of DR at an early stage. Before intravitreal injection, no fluorescent signals were detected in any of the groups. Six hours after the image probe injection, we found some strong fluorescent spots of VEGF expression in the DR model; the signal remained for 24 h, and then declined 72 h later. In contrast, no fluorescence signals were found in the normal retina. Without antibody labeling, the free FITC disappeared in the retina within 24 h, and no specific fluorescence was observed. Moreover, VEGF-positive fluorescent signals were automatically analyzed by image segmentation, which provided a more objective and precise approach for quantitative VEGF measurement. The *in vivo* imaging results imply that our molecular fluorescence-targeted imaging has the ability to dynamically locate and quantify VEGF relative expression in the retina.

Fluorescence molecular imaging can only provide two-dimensional planar imaging of VEGF expression in DR retina. It is more constructive if we can visualize the spatial distribution of VEGF expression in three dimensions and analyze the spatial correlation of VEGF expression

Biomedical Optics EXPRESS

with microvascular abnormalities in a DR model. Hence, image processing and analysis were further performed with *ex vivo* fluorescence imaging in this study. VEGF expression in 3D was characterized in terms of quantity, size, location, and spatial correlation with microvascular lesions. It is worth noting that the *ex vivo* imaging results analyzed by the medical image analysis not only supported our *in vivo* results, but also provided more detailed and interesting findings. First, our data revealed that VEGF expression in the retina mainly co-localized with DR lesions in the early NPDR stage, and there were more obvious VEGF-positive areas of fluorescence surrounding the dilated capillaries or areas of capillary closure, confirming that VEGF is already highly expressed in the early stage of NPDR. This is consistent with a previous study [21] that reported that the increased expression of VEGF precedes the onset of diabetic neovascularization [11,20,39]. In addition, western blotting, real-time polymerase chain reaction, and immunofluorescence staining also confirmed the overexpression of VEGF (Supplement 1, Fig. S2, A and B). Second, it is interesting to note that VEGF was generally abnormally expressed at the bifurcation of blood microvessels. This advances our knowledge that vascular lesions of DR in animal models may start from the vascular bifurcation, which is possibly due to the weak vascular connection there. In contrast, there was no specific binding of the probe found in the normal group. Third, we found that the retinal microvessels were incomplete in the diabetic model stained with EB, which may be due to pericyte apoptosis and the loosening of endothelial cells. Fourth, we provided evidence for the formation processes of IRMA, which are usually difficult to observe clinically. Multiple small microaneurysms fused to form a large microaneurysm, forming the early signs of IRMA, where high VEGF expression was detected.

Notably, most studies to date have focused on the detection of VEGF expression levels [40–42]. However, clinically, the distribution of VEGF is also a very important predictive marker, which is closely correlated with the anti-VEGF therapy response. A large number of studies have confirmed that there are two types of angiogenesis: physiological angiogenesis and pathological angiogenesis [42,43]. In the early stage of the disease, there is elevated expression of VEGF, which may promote physiological angiogenesis through a certain process [37–39]. Our experiment clearly found that in the early stage of NPDR, the first pathological sign was a large number of dilated capillaries with high VEGF expression. When retinal capillary endothelial damage occurred, a large number of VEGF-targeted probes could be observed binding to the outer surface of the vessel wall. Our results showed that there was accumulation of VEGF at the site of the bulging of the capillary wall. This may indicate that abnormally high VEGF levels indicate that microvessel capillaries change from physiological angiogenesis to irreversible pathological angiogenesis. This could also explain why in a series of clinical trials of anti-VEGF, repeated anti-VEGF treatment received no response, but micropulse laser therapy may be effective.

In conclusion, our study revealed that abnormally high VEGF expression can be quantitatively detected at the early stage of DR by using our developed ranibizumab-FITC probe in combination with fluorescence molecular imaging, which was further verified by both *in vivo* and *ex vivo* imaging (from 2D to 3D fluorescence imaging) using medical image analysis. Moreover, we established a correlation model between VEGF expression and microvessel abnormalities to provide a reference for the study of the DR model at an early stage. This *in vivo* fluorescence molecular imaging method for VEGF provides a promising way of distinguishing treatment responders from non-responders for anti-VEGF therapy and has a high possibility of being translated into clinical practice in the future.

Funding. National Natural Science Foundation of China (61771326, 61827809); Science and Technology Project of Beijing Municipal Commission of Education (KM202010025026).

Acknowledgments. The authors thank Prof. Minghui Kong, Dr. Zheqing Li, Prof. Xueqian Guo, Dr. Li Yan and Prof. Lin Hua for their kindly assistance in our experiments.

Disclosures. The authors declare no conflicts of interest.

Biomedical Optics EXPRESS

Data availability. Data underlying the results presented in this paper are not publicly available at this time but may be obtained from the authors upon reasonable request.

Supplemental document. See Supplement 1 for supporting content.

References

1. G. R. Dagenais, H. C. Gerstein, X. Zhang, M. McQueen, S. Lear, and P. Lopez-Jaramillo, "Variations in diabetes prevalence in low-, middle-, and high-income countries: results from the prospective urban and rural epidemiological study," Diabetes Care **39**(5), 780–787 (2016).
2. Y. Xu, L. Wang, J. He, Y. Bi, M. Li, and T. Wang, "Prevalence and control of diabetes in Chinese adults," JAMA **310**(9), 948–959 (2013).
3. J. W. Yau, S. L. Rogers, R. Kawasaki, E. L. Lamoureux, J. W. Kowalski, and T. Bek, "Global prevalence and major risk factors of diabetic retinopathy," Diabetes Care **35**(3), 556–564 (2012).
4. American Diabetes Association, "Standards of Medical Care in Diabetes-2020 Abridged for primary care providers," Clin Diabetes **38**(1), 10–38 (2020).
5. A.N. Kollias and M. W. Ulbig, "Diabetic retinopathy: early diagnosis and effective treatment," Dtsch Arztebl Int **107**(5), 75–83 (2010).
6. D. S. Ting, G. C. Cheung, and T. Y. Wong, "Diabetic retinopathy: global prevalence, major risk factors, screening practices and public health challenges: a review," Clinical & Experimental Ophthalmology **44**(4), 260–277 (2016).
7. C. J. Hippisley and C. Coupland, "Diabetes treatments and risk of amputation, blindness, severe kidney failure, hyperglycaemia, and hypoglycaemia: open cohort study in primary care," BMJ **352**, i1450 (2016).
8. J. A. Wells, A. R. Glassman, A. R. Ayala, L. M. Jampol, N. M. Bressler, and S. B. Bressler, "Aflibercept, bevacizumab, or ranibizumab for diabetic macular edema: two-year results from a comparative effectiveness randomized clinical trial," Ophthalmology **123**(6), 1351–1359 (2016).
9. B. P. Nicholson and A. P. Schachat, "A review of clinical trials of anti-VEGF agents for diabetic retinopathy," Graefes Arch. Clin. Exp. Ophthalmol. **248**(7), 915–930 (2010).
10. D. Ribatti, "The discovery of the fundamental role of VEGF in the development of the vascular system," Mechanisms of Development **160**, 103579 (2019).
11. N. Gupta, S. Mansoor, A. Sharma, A. Sapkal, J. Sheth, P. Falatoonzadeh, B. Kuppermann, and M. Kenney M, "Diabetic retinopathy and VEGF," TOOPHTJ **7**(1), 4–10 (2013).
12. M. Potente, H. Gerhardt, and P. Carmeliet, "Basic and therapeutic aspects of angiogenesis," Cell **146**(6), 873–887 (2011).
13. K. Brogan, M. Precup, A. Rodger, D. Young, and D. F. Gilmour, "Pre-treatment clinical features in central retinal vein occlusion that predict visual outcome following intravitreal ranibizumab," BMC Ophthalmol. **18**(1), 37 (2018).
14. O. A. Sorour, N. Mehta, C. R. Baumal, A. Ishibazawa, K. Liu, and E. K. Konstantinou, "Morphological changes in intraretinal microvascular abnormalities after anti-VEGF therapy visualized on optical coherence tomography angiography," Eye and Vis. **7**(1), 29 (2020).
15. R. L. Avery, A. A. Castellarin, N. C. Steinle, D. S. Dhoot, D. J. Pieramici, and R. See, "Systemic pharmacokinetics following intravitreal injections of ranibizumab, bevacizumab or aflibercept in patients with neovascular AMD," Br. J. Ophthalmol. **98**(12), 1636–1641 (2014).
16. E. Pearce, V. Chong, and S. Sivaprasad, "Aflibercept reduces retinal hemorrhages and intravitreal microvascular abnormalities but not venous beading: secondary analysis of the CLARITY study," Ophthalmology Retina **4**(7), 689–694 (2020).
17. Y. H. Aldebasi, A. H. Rahmani, A. A. Khan, and S. M. Aly, "The effect of vascular endothelial growth factor in the progression of bladder cancer and diabetic retinopathy," Int. J. Clin. Exp. Med. **6**(4), 239–251 (2013).
18. J. Lv, M.M. Chen, Z. H. Mu, F. Wang, Z. Y. Qian, and L. Zhou, "Intravitreal bevacizumab injection attenuates diabetic retinopathy in adult rats with experimentally induced diabetes in the early stage," Journal of Diabetes Research **2018**(5), 9216791 (2018).
19. H. Faatz, M. L. Farecki, K. Rothaus, M. Gutfleisch, D. Pauleikhoff, and A. Lommatzsch, "Changes in the OCT angiographic appearance of type 1 and type 2 CNV in exudative AMD during anti-VEGF treatment," BMJ Open Ophth. **4**(1), e000369 (2019).
20. P. A. Campochiaro, C. C. Wykoff, H. Shapiro, R. G. Rubio, and J. S. Ehrlich, "Neutralization of vascular endothelial growth factor slows progression of retinal nonperfusion in patients with diabetic macular edema," Ophthalmology **121**(9), 1783–1789 (2014).
21. M. Y. Hsu, S. J. Chen, K. H. Chen, Y. C. Hung, H. Y. Tsai, and C. M. Cheng, "Monitoring VEGF levels with low-volume sampling in major vision-threatening diseases: age-related macular degeneration and diabetic retinopathy," Lab Chip **15**(11), 2357–2363 (2015).
22. S. V. Schmitz, F. G. Holz, A. C. Bird, and R. F. Spaide, "Fundus autofluorescence imaging: review and perspectives," Retina **28**(3), 385–409 (2008).
23. T. E. Carlo, A. Romano, N. K. Waheed, and J. S. Duker, "A review of optical coherence tomography angiography (OCTA)," Int. J. Retina Vitreous **1**(1), 5 (2015).
24. I. S. Kornblau and J. F. El-Annan, "Adverse reactions to fluorescein angiography: a comprehensive review of the literature," Survey of Ophthalmology **64**(5), 679–693 (2019).

Biomedical Optics EXPRESS

25. E. Al Kahtani, Z. Xu, S. Al Rashaed, L. Wu, A. Mahale, J. Tian, E. B. Abboud, N. G. Ghazi, I. Kozak, V. Gupta, J. F. Arevalo, and E. J. Duh, "Vitreous levels of placental growth factor correlate with activity of proliferative diabetic retinopathy and are not influenced by bevacizumab treatment," Eye **31**(4), 529–536 (2017).
26. M. F. Cordeiro, L. Guo, V. Luong, G. Harding, W. Wang, H. E. Jones, S. E. Moss, A. M. Sillito, and F. W. Fitzke, "Real-time imaging of single nerve cell apoptosis in retinal neurodegeneration," Proceedings of the National Academy of Sciences **101**(36), 13352–13356 (2004).
27. J. H. Meyer, A. Cunea, K. Licha, P. Welker, D.B. Sonntag, and P. Wafula, "In vivo imaging of fluorescent probes linked to antibodies against human and rat vascular endothelial growth factor," Invest. Ophthalmol. Vis. Sci. **57**(2), 759–770 (2016).
28. P. Royle, H. Mistry, P. Auguste, D. Shyangdan, K. Freeman, and N. Lois, "Pan-retinal photocoagulation and other forms of laser treatment and drug therapies for non-proliferative diabetic retinopathy: systematic review and economic evaluation," Health Technol. Assess. **19**(51), 1–248 (2015).
29. M. Arima, D. Cui, T. Kimura, K. H. Sonoda, T. Ishibashi, and S. Matsuda, "Basigin can be a therapeutic target to restore the retinal vascular barrier function in the mouse model of diabetic retinopathy," Sci Rep **6**(1), 38445 (2016).
30. D. Sun, S. Nakao, F. Xie, S. Zandi, A. Bagheri, and M. R. Kanavi, "Molecular imaging reveals elevated VEGFR-2 expression in retinal capillaries in diabetes: a novel biomarker for early diagnosis," FASEB j. **28**(9), 3942–3951 (2014).
31. B. L. Furman, "Streptozotocin-induced diabetic models in mice and rats," Current Protocols in Pharmacology **70**(6), 1–5 (2015).
32. P. K. Sahoo and G. Arora, "A thresholding method based on two-dimensional Renyi's entropy," Pattern Recognition **37**(8), 1149–1161 (2014).
33. C. Campa, G. Alivernini, E. Bolletta, M. B. Parodi, and P. Perri, "Anti-VEGF therapy for retinal vein occlusions," CDT **17**(3), 328–336 (2016).
34. N. Papadopoulos, J. Martin, Q. Ruan, A. Rafique, M. P. Rosconi, and E. Shi, "Binding and neutralization of vascular endothelial growth factor (VEGF) and related ligands by VEGF Trap, ranibizumab and bevacizumab," Angiogenesis **15**(2), 171–185 (2012).
35. S. K. Blick, G. M. Keating, and A. J. Wagstaff, "Ranibizumab," Drugs **67**(8), 1199–1206 (2007).
36. S. Lien and H. B. Lowman, "Therapeutic anti-VEGF antibodies," Handb. Exp. Pharmacol. **181**(181), 131–150 (2008).
37. L. Q. García, R. A. Luaces, M. G. Martínez, G. C. Mondelo, O. Maroñas, and V. Mangas, "Pharmacokinetics of intravitreal Anti-VEGF drugs in age-related macular degeneration," Pharmaceutics **11**(8), 365 (2019).
38. R. L. Avery, A. A. Castellarin, N. C. Steinle, D. S. Dhoot, D. J. Pieramici, and R. See, "Systemic pharmacokinetics and pharmacodynamics of intravitreal aflibercept, bevacizumab, and ranibizumab," Retina **37**(10), 1847–1858 (2017).
39. D. R. Cha, Y. S. Kang, S. Y. Han, Y. H. Jee, K. H. Han, and J. Y. Han, "Vascular endothelial growth factor is increased during early stage of diabetic nephropathy in type II diabetic rats," J. Endocrinol. **183**(1), 183–194 (2004).
40. E. H. Sohn, S. He S, L. A. Kim, H. SalehI, M. Javaheri, and C. Spee, "Angiofibrotic response to vascular endothelial growth factor inhibition in diabetic retinal detachment: report no. 1," Arch. Ophthalmol. **130**(9), 1127–1134 (2012).
41. Z. Zhou, H. and Ju, M. Sun, and H. Chen, "Serum vascular endothelial growth factor levels correlate with severity of retinopathy in diabetic patients: a systematic review and meta-analysis," Disease Markers **2019**, 9401628 (2019).
42. A. Hoeben, B. Landuyt, M. S. Highley, H. Wildiers, A. T. Oosterom, and E. A. Bruijn, "Vascular endothelial growth factor and angiogenesis," Pharmacol. Rev. **56**(4), 549–580 (2004).
43. A. B. Stefano, D. Massihnia, F. Grisafi, M. Castiglia, F. Toia, and L. Montesano, "Adipose tissue, angiogenesis and angio-MIR under physiological and pathological conditions," European Journal of Cell Biology **98**(2-4), 53–64 (2019).